Delay Analysis and Buffer Sizing for Priority-Aware Networks-on-Chip

Baoliang Li[a,*], Zeljko Zilic[b], WenhuaDou[a]

[a]*College of Computer, National University of Defense Technology, Changsha 410073, P.R. China*
[b]*Department of Electrical & Computer Engineering, McGill University, Montreal H3A-2A7, Quebec, Canada*

Abstract

Priority-aware wormhole-switched NoC is promising to meet both the worst-case and average-case performance requirements of on-chip communication. To deploy real-time applications on this platform, the worst-case end-to-end delay and buffer requirement of this platform must be analyzed and guaranteed. In this paper, we first build a Real-Time Calculus (RTC) based performance model for the priority-aware wormhole-switched NoC. Based on this model, we then propose an end-to-end delay analysis algorithm and a buffer sizing algorithm. The delay analysis algorithm can give much tighter delay bound than the deterministic network calculus-based method, because it takes the maximum service capability and minimum arrival rate into consideration. The buffer sizing algorithm tries to reduce the buffer space required for each flow without violating the deadline constraint, which improves the backlog bound obtained by the link-level buffer-space analysis method. Both algorithms are topology-independent. Taking the architecture parameters and the flow specifications as input, they can give the end-to-end delay bound and buffer requirement of each flow. Our algorithms enable the fast performance evaluation and buffer allocation of priority-aware wormhole-switched NoCs, which can be used for application mapping, routing selection and power reduction, etc. The correctness of our performance model is verified by comparing with the simulation results.

Keywords: Networks-on-Chip (NoC), delay bound, buffer sizing

1. Introduction

Networks-on-Chip (NoC) is proposed to meet the strict and complex communication requirements of modern large-scale Chip-MultiProcessor (CMP) and System-on-Chip (SoC). Although various NoC proposals have emerged, most of

---

*Corresponding author. Tel: (514)692-3141
Email address: happybaoliang@gmail.com

them are designed to improve the average-case performance of on-chip interconnects. However, there are a variety of on-chip applications, which are sensitive to the worst-case communication performance of NoC. Designing the on-chip real-time communication infrastructure for these applications and analyzing its feasibility is a major challenge for researchers.

Although various hardware implementations have been proposed to meet the rigorous on-chip real-time communication requirement, e.g. Time-Division Multiplexing (TDM) [1], circuit-switch [2] and time-triggered switch [3], the average performance and resource utilization of these proposals are very poor. In contrast, wormhole-switched NoC is widely used in on-chip network due to its efficiency. Thus, providing real-time communication support on the conventional wormhole-switched NoC becomes the most promising solution to meet both average-case and worst-case communication requirements. A key step before the wormhole-switched NoC is adopted as the platform of real-time communication is to check whether the deadline constraints of all the real-time flows are met. An effective buffer analysis approach is also needed to optimize the buffer allocation under the real-time constraint, since the on-chip buffer usually contributes to a significant portion of the entire router's power and area [4, 5].

A tight worst-case delay and buffer requirement analysis is crucial for the application of wormhole switched NoCs in real-time communication, since an overoptimistic estimation will lead to the violation of the deadline, while an overly pessimistic estimation will make the utilization of on-chip resource very low. The conventional simulation-based method is not appropriate for this purpose, because the worst-case scenarios are difficult to be captured by simulation. As an alternative, analytical methods can establish the relationship between performance metrics and design parameters, and give the worst-case performance bounds. A great deal of research [6, 7, 8, 9, 10, 11, 13] focused on the analysis of worst-case delay bound and buffer requirement for the priority-aware wormhole-switched networks. Among all these analytical methods, the Link-Level Analysis (LLA) [7, 13] and the Deterministic Network Calculus (DNC) [8] based method outperform the others when the tightness of delay bound is considered. The LLA assumes that the packets arrive periodically or sporadically, and the buffer size is sufficiently large to eliminate the influence of flow control on the delay bound. The DNC based method [8] overcomes these two limitations by utilizing two general concept, i.e. service curve and arrival curve, to characterize the minimum service capability and maximum arrival rate, and deriving the worst-case performance bound by applying the advanced operators and properties of the DNC theory. However, the delay bound obtained by the DNC method [8] can be further improved if the maximum service capability of routers and the minimum arrival rate of traffic are taken into consideration.

In this paper, we try to improve the delay bound and buffer requirement derived by the DNC [8] and LLA [13] method. The theoretical framework of our performance model is the Real-Time Calculus (RTC) [12], which is originally used for the schedulability analysis of real-time system. To the best of our knowledge, it is the first time that this theory is used to model and analyze the performance of NoCs. The reason we choose RTC lies in the fact that it is

the extension of DNC theory, which integrates the maximum service capability and minimum arrival rate to characterize more detailed information about the traffic and service process. The main contribution of this paper is three-fold: (1) We construct a novel performance model for the priority-aware wormhole-switched NoC with credit-based flow control. (2) We propose an end-to-end delay analysis algorithm for the priority-aware wormhole-switched NoC based on our performance model. The delay bound obtained by our algorithm is much tighter than the DNC method [8]. (3) We propose a buffer sizing algorithm based on the constructed performance model. This algorithm considers the impact of flow control on the delay bound, and allocates just enough buffer space at each router for the flows to meet their deadline. When applied to guide the buffer allocation of priority-aware wormhole-switched NoCs, our algorithm can save more buffer space than the Link-Level Buffer-space Analysis (LLBA) method [13]. Our delay analysis and buffer sizing algorithms can be used for the design space exploration, IP core mapping, task mapping, routing selection, etc.

The rest of this paper is organized as follows: we present the existing real-time communication proposals and its related performance analysis methods in Section 2. In Section 3, the basic assumptions on priority-aware wormhole-switched NoC and a brief introduction to the RTC theory are presented. The detailed modeling process is presented in Section 4, where we also propose the end-to-end delay analysis algorithm and buffer sizing algorithm. We present the comparison results with simulation and other analytical methods in Section 5. Finally, we summarize our paper in Section 6.

2. Related Work

Since introduction in 2001 [14], NoC is designed to be either best-effort or guaranteed-service to meet different on-chip communication requirements. Best-effort NoC can make better use of the on-chip shared resource, but it does not necessarily provide any performance guarantee for the applications. To provide the guaranteed services for different applications, a simple and effective solution is to classify these applications into several service classes, each with different priorities, and the network provides services according to the priority of each class. Representative implementations of this idea include QNoC [15], fixed-priority NoC [6] and Æthereal [1] etc. The performance evaluation method the guaranteed service NoC include the average-case analysis and worst-case analysis. For the average-case analysis, simulation and analytical methods hold the dominant position. However, for the worst-case analysis, simulation is not sufficient due to the difficulty in covering all the corner cases.

The worst-case performance bound of the priority-aware wormhole-switched networks has been extensively studied in literature. In [9], the contention tree model was proposed to analyze the feasibility of real-time traffic delivered by priority-aware wormhole-switched NoC. It improves the previous results, e.g. lumped link model [10] and dependency graph model [11], by allowing the concurrent link usage. The Flow-Level Analysis (FLA) proposed in [6] improves the results obtained by contention tree model [9], lumped link model [10] and

3

dependency graph model [11]. A comprehensive comparison between FLA and the other method can be found in [16], in which several defects of the previous method are illustrated and the advantages of FLA are highlighted. The LLA [7] improves the FLA by analyzing each link segment separately. Two buffer sizing methods based on FLA and LLA, i.e. Flow-Level Buffer-space Analysis (FLBA) and Link-Level Buffer-space Analysis (LLBA), are proposed in [13] to estimate the buffer size of priority-aware wormhole-switched NoC. Both FLA and LLA assume that the traffic arrives periodically or sporadically, and that routers have sufficiently large buffer size, which is a significant simplification to the realistic traffic pattern and router implementation. In addition, the FLBA and LLBA can only compute the minimum buffer size at each router to avoid the back-pressure caused by flow control. We can further reduce the buffer size as long as the deadline constraint is not violated.

On the other hand, although the DNC based performance model for best-effort NoC proposed in [17] can also be applied to the analysis of priority-aware wormhole-switched NoC, the obtained performance bounds are very conservative, especially for the high-priority flows. This is because the model does not take the priority into consideration. To overcome this limitation, a revised DNC performance model was proposed to analyze the worst-case delay of priority-aware wormhole-switched NoC in [8]. We found that the DNC method in [8] can be further improved if we take the maximum service capability of each router and minimum arrival rate of each flow into consideration. Motivated by this observation, we adopt the RTC theory [12] to build the worst-case performance model for the priority-aware wormhole-switched NoC. Real-time calculus extends the DNC theory [18] by integrating the minimum arrival curve and maximum service curve to characterize more detailed information about the traffic and service processes. Due to its ability of analyzing complex system, RTC has been widely used in the modeling and analysis of Controller Area Networks [19], FlexRay [20], etc. To ease the application of RTC, a toolbox has been implemented in [21] to support the numerical calculation.

3. Preliminaries

3.1. Basic Assumptions

In this paper, the priority-aware NoC is represented as a directional network topology graph $G : V \times E$, where V and E represent the set of routers and links respectively. Each link $e_{i,j} \in E$ corresponds to a physical channel connecting the two routers R_i and R_j. A flow is a sequence of packets with the same transmission path, source address and destination address. Packet of different flows generated by a Intellectual Property (IP) core are buffered at different queues within the corresponding Network Interface (NI). Each packet is comprised of one head flit, one tail flit and several body flits. The path of a flow f_i traversed is defined as a router chain starting from the injection router (denoted as $start_i$) and ending at the ejection router (denoted as end_i). The set of all the flows in the network is denoted as $\mathcal{F}$, and each flow $f_i \in \mathcal{F}$ has a fixed-priority P_i and

4

deadline D_i. The set of routers along the path of f_i is denoted as $\mathcal{R}_i$, and the set of links a flow f_i traversed is denoted as Γ_i. There exists contention between flow f_i and f_j, if and only if $\Gamma_i \wedge \Gamma_j \neq \emptyset$. For router R_j along the path of flow f_i, denote the set of contending flows at R_j sharing the same priority with f_i as Θ_{R_j,f_i}, the set of contending flows at R_j with lower priorities than f_i as Ω_{R_j,f_i}, and the buffer size reserved at R_j for f_i as B_{R_j,f_i}.

The router we considered is the priority-aware wormhole-switched router proposed in [6] and further discussed in [22][10][7]. Each router has the same number of input and output ports, and each input port have sufficient Virtual Channel (VC) to accommodate all the incoming packets of different priority levels. The allocation of VC is determined by the VC allocator. The buffer depth of each VC is finite, and the credit-based flow control [23] is adopted between adjacent routers to prevent buffer overflow. To ensure the predicable transmission delay, a deterministic routine computation module is used to determine the output port of each packet. The crossbar is utilized to switch traffic from input ports to the output ports, and the switch operation is determined by the switch allocator. The switch allocator is priority-aware, if multiple flits from different input ports or different VCs of the same input port contend for the same output port, it will only grant the flit with the highest priority. Flits from a lower priority can transmit a flit, if and only if there are no contending flits from higher priority or the higher-priority flits are self-blocked due to the insufficiency of VC buffer at the downstream router.

The micro-architecture of the priority-aware router considered in this paper has standard pipeline stages, i.e. Buffer-Write (BW), Route Computation (RC), VC Allocation (VA), Switch Allocation (SA), Switch Traversal (ST) and Link Traversal (LT). For the detailed description, please refer to [24]. Each head flit should go through all these stages to determine the path and reserve a VC for the following non-head flits. Non-head flits skip the RC and VA stages since the routine and VC have been determined by the head flit. Router resource and control information reserved for a packet will be released only after the tail flit of the packet has departed from the router. An additional priority field in the head flit is required for the routers to schedule multiple contending flows according to their priority. Although we focus on standard router, our method can be easily modified to support other router micro-architecture, e.g. single-cycle router [22][6][10][7] and speculation-based router [24]. We will demonstrate the adoption of our model in a single-cycle router in subsection 5.1. To simplify our analysis, we also assume that the entire chip is synchronous, with clock frequency f and period T. Our method can also be applied to analyze Global Asynchronous Local Synchronous (GALS) NoC with little modification, because the routers located in different voltage-frequency islands can be synchronized with a half cycle synchronizer [25], which can be abstracted as a fixed-latency element in DNC theory [18].

Our performance model is topology-independent, but to demonstrate the basic idea, we take the mesh topology shown in Fig. 1 as an example throughout this paper. Routers in the mesh topology have five input/output ports, corresponding to the four cardinal directions (West, East, North and South)
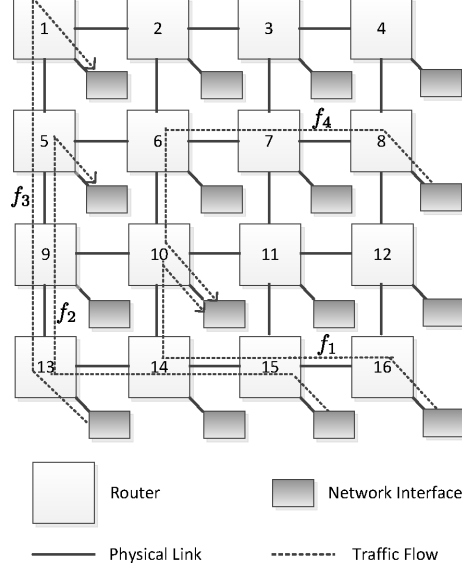
Figure 1: Mesh topology with four real-time traffic flows.

and the Local IP core. Although there are only four flows, i.e. f_1, f_2, f_3 and f_4, in the network, it is sufficient to demonstrate the idea of our method, and our method can handle more traffic flows efficiently. Our method extends the methods in [7][8] to allow multiple flows to share the same priority. Flits of different flows sharing the same priority are served in round-robin order when they compete the same output port. Since the minimum transmission unit in the priority-aware wormhole-switched NoC is flit and a high-priority flit can preempt the transmission of a low-priority flit, the NoC architecture considered in this paper is flit-level preemptive [26].

3.2. Introduction to Real-Time Calculus

Real-time calculus [12] is the extension of the DNC theory [18], by adding the upper service curve and lower arrival curve to describe the maximum service capability of a system and the minimum arrival rate of a event stream. Due to the space limitation, we only present the definitions of the RTC arrival curve and service curve in this subsection. For more details, please refer to [12].

Definition 1 (Real-Time Arrival Curve [12]). Denote by $R[s,t]$ the number of events within the time interval $[s,t]$. The lower and upper bounds on $R[s,t]$ are called the lower arrival curve α^l and upper arrival curve α^u, which satisfy

$$\alpha^l(t-s) \leq R[s,t] \leq \alpha^u(t-s), \forall s < t$$

and $\alpha^l(0) = \alpha^u(0) = 0$. The RTC arrival curve for a event stream is denoted as $< \alpha^l, \alpha^u >$ for short.

6

Definition 2 (Real-Time Service Curve [12]). Denote by $S[s,t)$ the number of events that can be processed by the system in time interval $[s,t)$. The lower and upper bounds on $S[s,t)$ are called the lower service curve β^l and upper service curve β^u, which satisfy

$$\beta^l(t-s) \leq S[s,t) \leq \beta^u(t-s), \forall s < t$$

and $\beta^l(0) = \beta^u(0) = 0$. The RTC service curve for a system is denoted as $< \beta^l, \beta^u >$ for short.

From these two definitions, we find that the upper arrival curve and lower service curve correspond to the arrival curve and service curve of DNC theory [18]. Similarly, the upper service curve corresponds to the maximum service curve of DNC theory. Thus, the two concatenation theorems for service curve (see Theorem 1.46 in [18]) and maximum service curve (see Theorem 1.6.1 in [18]) together form the concatenation theorem for the RTC service curve. Assume an event stream traverses two systems S_1 and S_2 in sequence, and S_i offers an RTC service curve $< \beta_i^l, \beta_i^u > (i = 1, 2)$ to this event stream. The concatenation theorem can give the equivalent RTC service curve offered by these two systems to the event stream, which is $< \beta_1^l \otimes \beta_2^l, \beta_1^u \otimes \beta_2^u >$.

In this paper, we will utilize the discrete time RTC arrival curve and service curve to characterize the arrived traffic and service capability of the wormhole-switched NoC, since the minimum time unit of this system is the clock period T. Events in the definitions of arrival curve and service curve refer to the arrival and service of flits, respectively. If we obtain the arrival curve $< \alpha^l, \alpha^u >$ of a specific flow at specific router and the service curve $< \beta^l, \beta^u >$ provided by this router, we can get the output arrival curve $< \alpha^{l'}, \alpha^{u'} >$ of this flow and leftover service curve $< \beta^{l'}, \beta^{u'} >$ of this router with the following equations [12]:

$$\alpha^{l'} = \min\{(\alpha^l \oslash \beta^u) \otimes \beta^l, \beta^l\} \tag{1}$$

$$\alpha^{u'} = \min\{(\alpha^u \otimes \beta^u) \oslash \beta^l, \beta^u\} \tag{2}$$

$$\beta^{l'} = (\beta^l - \alpha^u) \bar{\otimes} 0 \tag{3}$$

$$\beta^{u'} = \max\{(\beta^u - \alpha^l) \bar{\oslash} 0, 0\} \tag{4}$$

where $\otimes, \oslash, \bar{\otimes}, \bar{\oslash}$ correspond to the min-plus convolution, min-plus de-convolution, max-plus convolution and max-plus de-convolution [18].

After obtaining the arrival curve $< \alpha_f^l, \alpha_f^u >$ of flow f and the equivalent service curve $< \beta_f^l, \beta_f^u >$ offered by the system to flow f, we can get the delay bound by the following equation [18]

$$Delay(f) = H(\alpha_f^u, \beta_f^l) \tag{5}$$

where operator $H(\cdot, \cdot)$ computes the maximal horizontal deviation between its two operands.

4. Delay Analysis and Buffer Sizing

In this section, we first build an RTC based performance model for the priority-aware wormhole-switched NoC. Based on this performance model, we then propose an end-to-end delay analysis algorithm and a buffer sizing algorithm.

The performance model comprises two parts, i.e. traffic model and service model. The traffic model utilizes the RTC arrival curve to describe the arrival process of each flow. We will introduce two methods to obtain the arrival curve in subsection 4.1. The service model characterizes the services offered by the priority-aware NoC to each flow. The construction of the service model is much more complicated than the traffic model, and the following three issues should be considered while constructing the service model: (1) The path which head flit and non-head flits traverse are different. Only the head flit needs to traverse the RC and VA stage of a router, because the non-head flits of a packet follow the data-path built by the head flit. To simplify our service model, we need a special mechanism to characterize the service offered to head and non-head flits in a unified way. (2) Our performance model supports priority sharing among flows. Thus, the leftover service curve provided to the lower-priority flows can be derived only when all the service curves of high-priority flows have been computed. (3) The cyclic-dependence between the adjacent routers caused by flow control prevent us from deriving the end-to-end delay bound with Eq.(5), since the RTC theory is generally applicable to the feed-forward system. Thus, we should first break this cyclic-dependence before analyzing the performance bound. We will discuss the first two issues in subsection 4.2, and the last issue is discussed in subsection 4.3. Finally, we present the delay analysis algorithm and buffer sizing algorithm in subsection 4.4 and subsection 4.5, respectively.

4.1. Traffic Model

The communication in priority-aware wormhole-switched NoC is realized by transmitting packets, and the packet is divided into flits, which is the minimum transmission unit. Denote by $< \alpha^l(\Delta), \alpha^u(\Delta) >$ the flit arrival curve of a flow, namely, the minimum and maximum number of flits can be seen within any time window of length Δ. We can extract the flit arrival curve from the synthetic traffic or communication trace with the sliding window method [12]. For each window length Δ, this method tries to find the maximal and minimal number of arrived flits (corresponding to $\alpha^l(\Delta)$ and $\alpha^u(\Delta)$) by analyzing the time series of flits. However, the obtained flit arrival curve can only be applied to compute the worst-case performance bound at the flit level, because the service model we constructed in the following subsection characterizes the services provided by the system at the flit level. To obtain the packet level delay bound, this arrival curve must be L-packetized [18]. Denote by $L(n)$ the cumulative packet length (in flits) of the first n packets in a flow, $R(t)$ the cumulative arrived flits by time t. Then, the L-packetizer operator $\mathcal{P}^l(\cdot)$ is defined
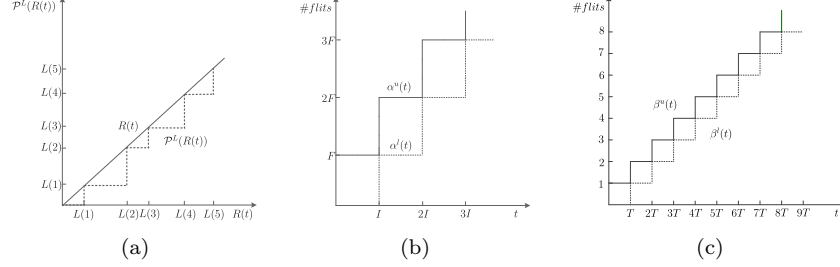
8

Figure 2: Traffic model and service model. (a) Definition of $\mathcal{P}^L(R(t))$. Cumulative arrival function $R(t)$ and the L-packetized cumulative arrival function $\mathcal{P}^L(R(t))$ are represented by the solid line and dotted line, respectively. (b) Real-time calculus arrival curve for periodically arrived traffic with period I and packet length F. The solid line and dotted line represent the upper arrival curve and lower arrival curve. (c) Service model for each pipeline stage. The solid lines and dotted lines represent the upper service curves and lower service curves, respectively.

as $\mathcal{P}^L(R(t)) = \sup\limits_{n\in\mathcal{N}}\{L(n)1_{L(n)\leq R(t)}\}^1$. Intuitively, $\mathcal{P}^l(\cdot)$ can be interpreted as the largest cumulative packet length contained in $R(t)$, as shown in Fig. 2a. For any flit arrival curve $< \alpha^l(\Delta), \alpha^u(\Delta) >$, the L-packetized arrival curve can be obtained by applying the following theorem.

Theorem 1 (L-packetized arrival curve). *Suppose a flow has a flit arrival curve $< \alpha^l(\Delta), \alpha^u(\Delta) >$, and the maximum packet length (in flits) of this flow is l_{max}. Then, it has an L-packetized arrival curve $< \alpha^l(\Delta)-l_{max}1_{\{\Delta>0\}}, \alpha^u(\Delta)+l_{max}1_{\{\Delta>0\}} >$.*

PROOF. For $\forall t \geq 0, \Delta \geq 0$, according to the basic properties of L-packetizer [18], we have

$$R(t) - l_{max} < \mathcal{P}^L(R(t)) \leq R(t)$$

and

$$R(t + \Delta) - l_{max} < \mathcal{P}^L(R(t + \Delta)) \leq R(t + \Delta).$$

The inequalities above indicate

$$R(t + \Delta) - R(t) - l_{max} < \mathcal{P}^L(R(t + \Delta)) - \mathcal{P}^L(R(t))$$

and

$$\mathcal{P}^L(R(t + \Delta)) - \mathcal{P}^L(R(t)) < R(t + \Delta) - R(t) - l_{max}.$$

Based on the definition 1, the L-packetized flow has a packet arrival curve $< \alpha^l(\Delta) - l_{max}1_{\{\Delta>0\}}, \alpha^u(\Delta) + l_{max}1_{\{\Delta>0\}} >$, which ends the proof. ∎

---

[1]$\mathcal{N}$ is the set of natural numbers and $1_{\{val\}}$ is the indicator function, $1_{\{val\}} = 1$ if and only if val is true.
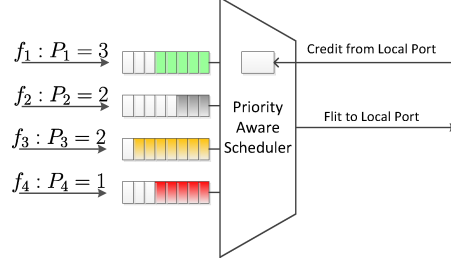
Figure 3: Structure of priority-aware network interface. Each flow has its dedicated buffer, and the scheduler selects the flit with the highest-priority for transmission at each cycle.

We can directly obtain the L-packetized arrival curve instead of transformation from flit arrival curve for some special cases. For example, suppose all the packets in a flow have the same length F and arrived periodically with period I. By applying the sliding window method [12], we can obtain the flit arrival curve of this flow, which is a pair of staircase functions[2] $< F \cdot u_{I,0}, F \cdot u_{I,I} >$. As shown in Fig. 2b, the obtained flit arrival curve which is equal to the L-packetized arrival curve $\mathcal{P}^L(\alpha)$, since $\mathcal{P}^L(R(t)) = R(t)$, $\mathcal{P}^L(\alpha^l(t)) = \alpha^l(t)$ and $\mathcal{P}^L(\alpha^u(t)) = \alpha^u(t)$.

4.2. Basic Feed-forward Service Model

The service model characterizes the service obtained by each flow along its transmission path, which will be discussed as follows.

4.2.1. Service Curve Provided by the Source NI

If an IP core generates more than one flow simultaneously, the source NI will schedule these flows to go through the output link according to their priorities. Figure 3 illustrates the internal structure of this priority-aware NI, where the IP core generates four flows simultaneously. Messages of different flows are encapsulated and stored in the dedicated buffer for that flow. The priority-aware scheduler selects one flit with the highest-priority at a time for transmission, and imposes an additional latency T to all the flits which traverse it. Therefore, the RTC service curve provided by the source NI (denoted as $< \beta^l_{NI}, \beta^u_{NI} >$) can also be obtained by applying the sliding window method [12], which is a pair of staircase functions $< u_{T,0}, u_{T,T} >$, as shown in Fig. 2c.

Given the set of flow specifications, Algorithm 1 can derive the service curve obtained by each flow at the source NI. The flow specification of f_i is a quadruple $(< \alpha^l, \alpha^u >, \mathcal{R}_i, D_i, P_i)$ that specifies the arrival curve, routine, deadline and priority of a flow.

---

[2]A staircase function $u_{T,\tau} = \lceil \frac{t+\tau}{T} \rceil$ for $t > 0$ and 0 otherwise, where $0 \leq \tau \leq T$ and $\lceil \cdot \rceil$ is the ceiling operator.

10

Algorithm 1 Compute the service curve at source NI

Require: The set of flow specifications
Ensure: The service curve obtained by each flow
1: Group the flows with priority P_i into subset $\mathcal{F}_i$.
2: $\beta_{NI}^{l'} = \lfloor \frac{t}{T} \rfloor$; $\beta_{NI}^{u'} = \lceil \frac{t}{T} \rceil$.
3: **for** each $\mathcal{F}_i$ from highest priority to lowest priority **do**
4:     **for** each flow $f_j \in \mathcal{F}_i$ **do**
5:         $\beta_{NI,f_j}^{l} = \lfloor \frac{\beta_{NI}^{l'}}{|\mathcal{F}_i|} \rfloor$; $//|\mathcal{F}_i|$ denotes the cardinality of $\mathcal{F}_i$
6:         $\beta_{NI,f_j}^{u} = \lceil \frac{\beta_{NI}^{u'}}{|\mathcal{F}_i|} \rceil$.
7:     **end for**
8:     $\alpha^l = \sum_{f_j \in \mathcal{F}_i} \alpha_{f_j}^l$; $\alpha^u = \sum_{f_j \in \mathcal{F}_i} \alpha_{f_j}^u$;
9:     $\beta_{NI}^{l'} = (\beta_{NI}^{l'} - \alpha^u) \bar{\otimes} 0$; $\beta_{NI}^{u'} = \max\{(\beta_{NI}^{u'} - \alpha^l) \bar{\oslash} 0, 0\}$.
10: **end for**

4.2.2. Service Curve Provided by the Router

While modeling the service capability of a router with RTC, we can analyze the data-path of a flow in the router stage-by-stage. Once we obtain the service curves offered by each stage, the service curve provided by the router to a flow can be derived by concatenating all these service curves. This is significantly different from the existing DNC based model [17, 8], where they treat the entire router as a whole and designate a Latency-Rate (LR) service curve [18] to simplify the performance bounds derivation. Whereas, our model uses the staircase functions to characterize the detailed behavior of this discrete time system. The advantage of our method is that, it can be easily modified to characterize the non-standard router micro-architectures, by simply letting the service curve of non-existed stages to be a burst delay function $\delta_0(t)$[3]. Next, we try to derive the service curves of all these stages:

(1) BW stage, SA stage and LT stage: all the flits within a traffic flow will go through these three stages, and experience a fixed delay T at each stage. The service curves provided by these stages, i.e. $< \beta_{BW}^l, \beta_{BW}^u >$, $< \beta_{SA}^l, \beta_{SA}^u >$ and $< \beta_{LT}^l, \beta_{LT}^u >$, can be derived by applying the sliding window method [12], which are the same as the service curve of source NI, as shown in Fig. 2c.

(2) RC stage and VA stage: the latency of head flit experienced at these two stages is T. Although the non-head flits do not go through these two stages, they have to wait for at most two cycles before entering the SA stage, e.g. the first three body flits of a packet shown in Fig. 4. Thus, a sophisticated solution to construct a unified lower service curve for head flit and non-head flits at these two stages comes from viewing each of these two stages impose an additional delay T for all the flits. Thus, the equivalent lower service curve of these two stages, i.e. β_{RC}^l and β_{VA}^l, can be obtained by applying the sliding window

---
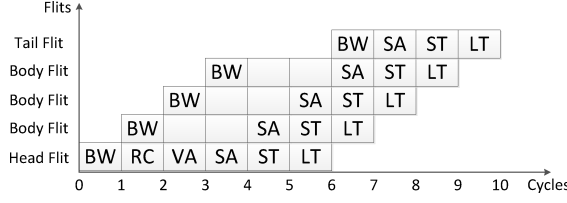[3]$\delta_{val}(t) = +\infty$ if $t > val$, and 0 otherwise.

Figure 4: Time-line graph of a packet going through the standard router pipeline. The delayed tail flit enters the ST stage immediately after it is written into the dedicated buffer.

method [12], which are equal to the staircase function $u_{T,0}(t)$. To derive the upper service curve of these two stages, let us consider the most 'lucky' flits of a flow, e.g. the tail flit shown in Fig. 4. This flit can enter the SA stage immediately after it was written into the dedicated VC buffer. For this case, the RC and VA stages impose a zero latency to it. Thus, we can utilize the burst delay function $\delta_0(t)$ to represent the upper service curve of these two stages.

(3) ST stage: each output port of the wormhole-switched NoC has a switch allocator to schedule the switch traversal among all the contending flows at each clock cycle. The notation $< \beta^l_{ST,R^p_i}, \beta^u_{ST,R^p_i} >$ is used to identify the service curve obtained by all the contending flows injected into switch port p. For the mesh topology, let the port indicator p be W (West port), E (East port), S (South port), N (North port) or L (Local port). Thus, Following the same procedure as BW stage, we can get the service curves provided to all the contending flows, which is $< u_{0,T}(t), u_{T,T}(t) >$, as shown in Fig. 2c.

It can be found that the contention of different flows within a router only might occur at ST stage. For the fixed-priority scheduling policy, switch allocators schedule the flow with the highest priority first, flows with the same priority will be served with round-robin order. All the unscheduled flows will impose an additional latency T due to the failure of switch arbitration.

Denote by $< \beta^l_{ST,R^p_i}, \beta^u_{ST,R^p_i} >$ the total service curve provided by the ST stage, $< \beta^l_{ST,R_i,f_j}, \beta^u_{ST,R_i,f_j} >$ the service curve provided to flow f_j by ST stage of router R_i, and $< \beta^{l'}_{ST,R^p_i}, \beta^{u'}_{ST,R^p_i} >$ the leftover service curve after serving the flows with higher priority than f_j. In order to obtain the service curve $< \beta^l_{ST,R_i,f_j}, \beta^u_{ST,R_i,f_j} >$, we should consider the following two cases:

(a) All the flows contending with f_j at R_i have lower priorities than f_i. For the synchronized router architecture, flow f_j gets the total service curve $< \beta^{l'}_{ST,R^p_i}, \beta^{u'}_{ST,R^p_i} >$.

(b) There exists some contention flows with the same priority as f_j. Since all the flows in Θ_{R_i,f_j} got serviced in round-robin order, the service curve provided to f_j is $< \lfloor \beta^{l'}_{ST,R^p_i}/(|\Theta_{R_i,f_j}| + 1) \rfloor, \lceil \beta^{u'}_{ST,R^p_i}/(|\Theta_{R_i,f_j}| + 1) \rceil >$. After serving all the flows in Θ_{R_i,f_j}, the leftover service curve for low-priority flows can be derived by applying Eq.(3) and Eq.(4).

12

After we obtained the service curve provided by ST stage to flow f_j, we can get the service curve of the router directly. The equivalent feed-forward service curve of router R_i provided to f_j, i.e. $< \beta^l_{R_i,f_j}, \beta^u_{R_i,f_j} >$, can be obtained by concatenating the service curves of all these stages together:

$$\beta^l_{R_i,f_j} = \beta^l_{BW} \otimes \beta^l_{RC} \otimes \beta^l_{VA} \otimes \beta^l_{SA} \otimes \beta^l_{ST,R_i,f_j},$$
$$\beta^u_{R_i,f_j} = \beta^u_{BW} \otimes \beta^u_{RC} \otimes \beta^u_{VA} \otimes \beta^u_{SA} \otimes \beta^u_{ST,R_i,f_j}.$$

4.3. Feedback Service Model

To this end, we have constructed the traffic model and the feed-forward service model. The credit-based flow control introduces cyclic-dependence be-
tween the adjacent routers, and leads to self-blocking within a flow due to the insufficiency of buffer space at the downstream router. The cyclic-dependence between the adjacent routers prevents us from deriving the performance bound directly even after we have obtained the service curve reserved at each router for the target flow. In existing literature, this cyclic-dependence is addressed by
fixed-point iteration [28] or transformation from marked dataflow graph [29].

In this subsection, we will try to tackle the same problem with another solution. Our solution is inspired by [17], where the authors abstract the flow control as a network element (called flow controller) providing a service curve (corresponding to the lower service curve of RTC theory). Then, this service
curve is obtained by applying some basic properties of DNC theory [18]. To make the discussion concrete, we take flow f_2 in Fig. 1 as an example. We also utilize the scheduling network model [12] in RTC theory to visualize the credit-based flow control and complex relationship among f_2 and the other flows, as shown in Fig. 5. We ignore flow f_4 and the flow control of the other flows
for brevity and clarity. We also assume that, all the destination IP cores can consume the arrived flits immediately, thus there is no flow control between the ejection router and destination NI. However, to prevent the buffer overflow, the flow control between source NI and injection router is necessary.

A flow in the wormhole-switched router with credit-based flow control will
be blocked if there is no credit available. We can treat the blocking of a flow caused by credit-insufficiency as traversing a virtual pipeline stage, called Flow Control (FC) stage, as shown in Fig. 5. The equivalent service curve for this virtual stage can be obtained by the following theorem, which enables us to break the cyclic-dependence caused by flow control and build a comprehensive
performance model for the wormhole-switched router.

Theorem 2. *Suppose that the router provides a feed-forward service curve $< \beta^l, \beta^u >$, and the physical link between two routers provides service curve $< \beta^l_{LT}, \beta^u_{LT} >$, the buffer size and credit feedback delay are denoted as B and σ, respectively. Then, the flow controller at the upstream router provides an*
equivalent service curve $< \overline{\beta^l \otimes \beta^l_{LT} \otimes \delta_\sigma + B}, \overline{\beta^u \otimes \beta^u_{LT} \otimes \delta_\sigma + B} >$, where $\bar{f}$ is the sub-additive closure[4] of f.

---

[4] $\bar{f} = \inf_{n \geq 0} \{ f^{(n)} \}$, where $f^{(n)}$ represents the nth-fold convolution of f and $f^{(0)}(t) = \delta_0(t)$.
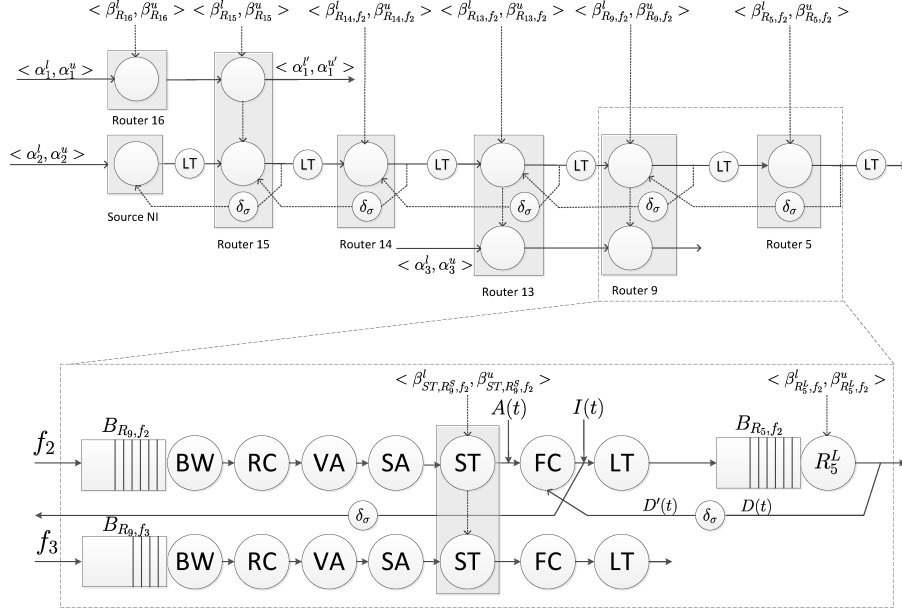
Figure 5: Scheduling network model for flow f_2

PROOF. We will take the flow controller between R_9 and R_5 in Fig. 5 as an example to derive the service curve of flow controller. Denote the amount of injected and departed flits at R_5 by time t as $I(t)$ and $D(t)$, and the amount of flits served by R_9 by time t as $A(t)$. The feedback link can be represented as a network element providing upper service curve $\delta_\sigma(t)$. The DNC service curve (i.e. lower service curve of RTC) has been derived in [17], which is $\overline{\beta^l \otimes \beta^l_{LT} \otimes \delta_\sigma + B_{R_5,f_2}}$.

In the rest of this proof, we will derive the upper service curve for the flow controller. For the flow control between router R_9 and R_5, we have $I(t) \leq A(t)$ for causality and $I(t) \leq D'(t) + B_{R_5,f_2}$ due to the effect of flow control, where $D'(t) \leq D \otimes \delta_\sigma(t)$. Thus,

$$I(t) \leq \min\{A(t), D'(t) + B_{R_5,f_2}\}.$$

Since the upper service curve corresponds to the maximum service curve in DNC theory [18], the following inequality holds by the definition of maximum service curve (see definition 1.6.1 in [18])

$$D(t) \leq I \otimes \beta^u_{LT}(t) \otimes \beta^u_{R_5,f_2}.$$

Bring $I(t)$ and $D'(t)$ into the above inequality, we get

$$
\begin{aligned}
D(t) &\leq & I \otimes \beta^u_{R_5,f_2} \otimes \beta^u_{LT}(t) \\
&\leq & \min\{A \otimes \beta^u_{R_5,f_2} \otimes \beta^u_{LT}(t), D \otimes \delta_\sigma \otimes \beta^u_{R_5,f_2} \otimes \beta^u_{LT}(t) + B\}.
\end{aligned}
$$

14

By applying Theorem 4.31 in [18], we have

$$D \leq A \otimes \beta^u_{R_5,f_2} \otimes \beta^u_{LT} \otimes \overline{\beta^u_{R_5,f_2} \otimes \beta^u_{LT} \otimes \delta_\sigma + B_{R_5,f_2}}.$$

Thus,

$$
\begin{aligned}
I & \leq & \min\{A, D' + B_{R_5,f_2}\} \\
& \leq & \min\{A, D \otimes \delta_\sigma + B_{R_5,f_2}\} \\
& \leq & \min\{A, A \otimes \beta^u_{R_5,f_2} \otimes \beta^u_{LT} \otimes \overline{\beta^u_{R_5,f_2} \otimes \beta^u_{LT} \otimes \delta_\sigma + B_{R_5,f_2}} \otimes \delta_\sigma + B_{R_5,f_2}\} \\
& = & \min\{A \otimes \delta_\sigma, A \otimes \overline{\delta_\sigma \otimes \beta^u_{R_5,f_2} \otimes \beta^u_{LT} + B_{R_5,f_2}}\} \\
& = & A \otimes \min\{\delta_\sigma, \overline{\beta^u_{R_5,f_2} \otimes \beta^u_{LT} \otimes \delta_\sigma + B_{R_5,f_2}}\} \\
& = & A \otimes \overline{\beta^u_{R_5,f_2} \otimes \beta^u_{LT} \otimes \delta_\sigma + B_{R_5,f_2}}
\end{aligned}
$$

where the steps from the third line to the fifth line hold due to the general properties of $\otimes$ operator (see Rule 6 and Rule 7 of Theorem 3.1.5 in [18]), and the last step follows from the definition of sub-additive closure.

The inequality $I \leq A \otimes \overline{\beta^u_{R_5,f_2} \otimes \beta^u_{LT} \otimes \delta_\sigma + B_{R_5,f_2}}$ implies that the flow controller at R_9 provides an upper service curve $\overline{\beta^u_{R_5,f_2} \otimes \beta^u_{LT} \otimes \delta_\sigma + B_{R_5,f_2}}$. Thus, we can conclude that for any router providing upper service curve β^u, the corresponding flow controller offers an upper service curve $\overline{\beta^u \otimes \beta^u_{LT} \otimes \delta_\sigma(t) + B}$. ∎

On obtaining the equivalent service curve of flow controller for f_i at router R_j (denoted as $< \beta^l_{FC,R_j,f_i}, \beta^u_{FC,R_j,f_i} >$), we get the equivalent service curve of router R_j after breaking the cyclic-dependence loop:

$$\beta^l_{R_j,f_i} = \beta^l_{BW} \otimes \beta^l_{RC} \otimes \beta^l_{VA} \otimes \beta^l_{SA} \otimes \beta^l_{ST,R_j,f_i} \otimes \beta^l_{FC,R_j,f_i},$$

$$\beta^u_{R_j,f_i} = \beta^u_{BW} \otimes \beta^u_{RC} \otimes \beta^u_{VA} \otimes \beta^u_{SA} \otimes \beta^u_{ST,R_j,f_i} \otimes \beta^u_{FC,R_j,f_i}.$$

Theorem 2 derives the RTC service curve of a single flow controller, and we can get the service curves of all the flow controllers along the router chain of any flow by applying Theorem 2 iteratively. As shown in Fig. 5, the service curve of a flow controller is determined by the service curves of the downstream flow controllers and routers. Hence, for each flow, we should compute the service curves of flow controllers from the ejection router to the source NI. Take flow f_2 as an example, we have $\beta^l_{FC,R_5,f_2}(t) = \delta_0(t)$ and $\beta^u_{FC,R_5,f_2}(t) = \delta_0(t)$ since there is no flow control between R_5 and destination NI. Then, we compute the service curve of flow controller at R_9 (i.e. $< \beta^l_{FC,R_9,f_2}, \beta^u_{FC,R_9,f_2} >$), which is $< \overline{\beta^l_{R_5,f_2} \otimes \beta^l_{LT} \otimes \delta_\sigma + B_{R_5,f_2}}, \overline{\beta^u_{R_5,f_2} \otimes \beta^u_{LT} \otimes \delta_\sigma + B_{R_5,f_2}} >$. By applying the concatenation theorem, we can obtain the equivalent service curve provided to f_2 by router R_9, which can be utilized to derive $< \beta^l_{FC,R_{13},f_2}, \beta^u_{FC,R_{13},f_2} >$ further. Following the same procedure, the service curve $< \beta^l_{FC,R_{14},f_2}, \beta^u_{FC,R_{14},f_2} >$, $< \beta^l_{FC,R_{15},f_2}, \beta^u_{FC,R_{15},f_2} >$ and $< \beta^l_{FC,NI,f_2}, \beta^u_{FC,NI,f_2} >$[5] can be derived.

---

[5]$< \beta^l_{FC,NI,f_2}, \beta^u_{FC,NI,f_2} >$ denotes the service curve of flow controller between source NI and injection router.

4.4. End-to-End Delay Analysis

In this subsection, we present the delay analysis algorithm, as shown in Algorithm 2. This algorithm takes the architecture parameters and flow specifications as input, and gives the worst-case end-to-end delay for all the flows. The architecture parameters specify the network topology graph, buffer size of each VC and the service curve of each pipeline stage. The flow specifications describes the arrival curve, routine, deadline and priority of each flow. The arrival curve of flow f_i at the source NI and ST stage of router R_j are denoted as $< \alpha^l_{f_i}, \alpha^u_{f_i} >$ and $< \alpha^l_{R_j,f_i}, \alpha^u_{R_j,f_i} >$, respectively. The leftover service curve of ST stage at output port p is represented as $< \beta^{l'}_{ST,R_j^p}, \beta^{u'}_{ST,R_j^p} >$ (Initially, let $\beta^{l'}_{ST,R_j^p} = \beta^l_{ST,R_j^p}$ and $\beta^{u'}_{ST,R_j^p} = \beta^u_{ST,R_j^p}$).

In the fixed-priority flit-level preemptive NoC, only the leftover service curve can be used by the low-priority flows. Thus, our algorithm compute the leftover service curve and delay bound from high-priority flows to low-priority flows. For each iteration, it performs the following four steps in sequence: (1) Calculating the service curves provided by the routers (lines 6-7) and flow controllers (lines 8-9) along the path. (2) Computing the worst-case end-to-end delay of the flow (lines 11-15), where the service curve provided by the source NI to f_i, i.e. $< \beta^l_{NI,f_i}, \beta^u_{NI,f_i} >$ has been computed with Algorithm 1. (3) The highlights of performance model when compared with the LLA method [7] and DNC method [8] is that our algorithm supports the priority-sharing. Thus, the leftover service curve at each router for low-priority flows can only be calculated when all the flows sharing the same priority have been calculated. To calculate the leftover service curve at ST stage, we have to first derive the equivalent service curve from source NI to R_j (lines 21-22) and the arrival curve at R_j (lines 24-25). Then, derive the leftover service curve with the aggregate arrival curve of the same priority-level (lines 26-31). The overall algorithm has two-level embedded loops, and the computation complexity for this algorithm is $O(HN)$, where N and H is the number of flows and the hop count of each flow. This algorithm can be easily implemented in the RTC toolbox [21] to compute the end-to-end delay bound automatically. Since our algorithm takes the upper service curve and lower arrival curve into consideration, our algorithm can give much tighter delay bound than the DNC-based delay analysis algorithm proposed in [8].

4.5. Buffer Sizing

The priority-aware wormhole-switched NoC [6, 11, 22] requires the same amount of VCs as the priorities to prevent priority inversion, which refers to the blocking of high-priority flows when the low priority flows occupy all the VCs [10]. To reduce the buffer area and power consumption of priority-aware wormhole-switched NoC, priority sharing [30] and buffer optimization [13] techniques have been proposed. However, the backlog bound of each router derived in [13] is the minimum buffer size that does not trigger the flow control. Reducing this buffer size further will cause the back-pressure between adjacent routers and lead to a larger end-to-end delay. However, it is allowed to do so as long

16

Algorithm 2 End-to-end delay analysis algorithm

Require: Architecture parameters and flow specifications
Ensure: Worst-case end-to-end delay for all the flows
1: **for** each flow $f_i \in \mathcal{F}$ with priority order **do**
2:     // Compute the service curve at each router for f_i
3:     $\beta_\tau^l = \delta_0(t)$;
4:     $\beta_\tau^u = \delta_0(t)$;
5:     **for** each router $R_j \in \mathcal{R}_i$ from end_i to $start_i$ **do**
6:         $\beta_{R_j,f_i}^l = \beta_{BW}^l \otimes \beta_{RC}^l \otimes \beta_{VA}^l \otimes \beta_{SA}^l \otimes \lfloor \frac{\beta_{ST,R_j^p}^{l'}}{|\Theta_{R_j,f_i}|+1} \rfloor \otimes \beta_\tau^l$;
7:         $\beta_{R_j,f_i}^u = \beta_{BW}^u \otimes \beta_{RC}^u \otimes \beta_{VA}^u \otimes \beta_{SA}^u \otimes \lceil \frac{\beta_{ST,R_j^p}^{u'}}{|\Theta_{R_j,f_i}|+1} \rceil \otimes \beta_\tau^u$;
8:         $\beta_\tau^l = \overline{\beta_{R_j,f_i}^l \otimes \beta_{LT}^l \otimes \delta_\sigma(t) + B_{R_j,f_i}}$;
9:         $\beta_\tau^u = \overline{\beta_{R_j,f_i}^u \otimes \beta_{LT}^u \otimes \delta_\sigma(t) + B_{R_j,f_i}}$;
10:     **end for**
11:     $\beta_{FC,NI,f_i}^l = \beta_\tau^l$;
12:     $\beta_{FC,NI,f_i}^u = \beta_\tau^u$;
13:     // Compute the end-to-end delay for f_i
14:     $\beta_{f_i} = \beta_{NI,f_i}^l \otimes \beta_{FC,NI,f_i}^l \otimes (\bigotimes_{R_k \in \mathcal{R}_i} (\beta_{R_k,f_i}^l \otimes \beta_{LT}^l))$;
15:     $Delay(f_i) = H(\alpha_{f_i}^u, \beta_{f_i})$;
16:     // Compute the leftover service curve for low-priority flows
17:     $\beta_{f_i}^l = \beta_{NI,f_i}^l \otimes \beta_{FC,NI,f_i}^l$;
18:     $\beta_{f_i}^u = \beta_{NI,f_i}^u \otimes \beta_{FC,NI,f_i}^u$;
19:     **for** $\forall R_j \in \mathcal{R}_i$ from $start_i$ to end_i **do**
20:         **if** $\Omega_{R_j,f_i} \neq \emptyset$ **then**
21:             $\beta^l = \beta_{f_i}^l \otimes \beta_{BW}^l \otimes \beta_{RC}^l \otimes \beta_{VA}^l \otimes \beta_{SA}^l$;
22:             $\beta^u = \beta_{f_i}^u \otimes \beta_{BW}^u \otimes \beta_{RC}^u \otimes \beta_{VA}^u \otimes \beta_{SA}^u$;
23:             //Compute the arrival curve of f_i at R_j
24:             $\alpha_{R_j,f_i}^l = \min\{(\alpha_{f_i}^l \oslash \beta^u) \otimes \beta^l, \beta^l\}$;
25:             $\alpha_{R_j,f_i}^u = \min\{(\alpha_{f_i}^u \otimes \beta^u) \oslash \beta^l, \beta^u\}$;
26:             **if** $Delay(f_k)$ has been calculated for $\forall f_k \in \Theta_{R_j,f_i}$ **then**
27:                 $\alpha_{R_j,f_i}^l = \alpha_{R_j,f_i}^l + \sum_{f_k \in \Theta_{R_j,f_i}} \alpha_{R_j,f_k}^l$;
28:                 $\alpha_{R_j,f_i}^u = \alpha_{R_j,f_i}^u + \sum_{f_k \in \Theta_{R_j,f_i}} \alpha_{R_j,f_k}^u$;
29:                 $\beta_{ST,R_j^p}^{l'} = (\beta_{ST,R_j^p}^{l'} - \alpha_{R_j,f_i}^u) \bar{\oslash} 0$;
30:                 $\beta_{ST,R_j^p}^{u'} = \max\{(\beta_{ST,R_j^p}^{u'} - \alpha_{R_j,f_i}^l) \bar{\oslash} 0, 0\}$;
31:             **end if**
32:         **end if**
33:         $\beta_{f_i}^l = \beta_{f_i}^l \otimes \beta_{R_j,f_i}^l \otimes \beta_{LT}^l$;
34:         $\beta_{f_i}^u = \beta_{f_i}^u \otimes \beta_{R_j,f_i}^u \otimes \beta_{LT}^u$;
35:     **end for**
36: **end for**

---

as the deadline constraint of each flow is not violated. Thus, our buffer sizing algorithm tries to reduce the initial buffer size of each router iteratively until the end-to-end delay of a flow violates its deadline or the buffer size is equal to one. The initial buffer size to avoid flow control can be obtained by the following theorem.

Theorem 3. *Denote by $\beta^l_{R_j,f_i}$ the feed-forward lower service curve obtained at $R_j \in \mathcal{R}_i$ by flow f_i, β^l_{LT} the lower service curve provided by the physical link between two adjacent routers, B_{R_j,f_i} the VC buffer size reserved for f_i at R_j and σ the credit feedback delay. Then, for $\forall R_j \in \mathcal{R}_i$, the buffer size*

$$B_{R_j,f_i} = \lceil \inf\{B | \beta^l_{R_j,f_i} \otimes \beta^l_{LT} \otimes \overline{\beta^l_{R_j,f_i} \otimes \beta^l_{LT} \otimes \delta_\sigma(t) + B} \geq \beta^l_{R_j,f_i} \otimes \beta^l_{LT}\} \rceil$$

is large enough to avoid flow control.

PROOF. We take flow f_2 in Fig. 1 as an example to prove this theorem. As stated by Theorem 2, we have

$$\beta^l_{FC,R_9,f_2} = \overline{\beta^l_{LT} \otimes \beta^l_{R_5,f_2} \otimes \delta_\sigma + B_{R_5,f_2}}$$

and

$$
\begin{aligned}
\beta^l_{FC,R_{13},f_2} &= \overline{\beta^l_{LT} \otimes \beta^l_{R_9,f_2} \otimes \overline{\beta^l_{LT} \otimes \beta^l_{R_5,f_2} \otimes \delta_\sigma + B_{R_5,f_2}} \otimes \delta_\sigma + B_{R_9,f_2}} \\
&= \overline{(\beta^l_{LT} \otimes \beta^l_{R_9,f_2} \otimes \delta_\sigma + B_{R_9,f_2}) \otimes \overline{\beta^l_{LT} \otimes \beta^l_{R_5,f_2} \otimes \delta_\sigma + B_{R_5,f_2}}} \\
&= \overline{\beta^l_{LT} \otimes \beta^l_{R_9,f_2} \otimes \delta_\sigma + B_{R_9,f_2}} \otimes \overline{\beta^l_{LT} \otimes \beta^l_{R_5,f_2} \otimes \delta_\sigma + B_{R_5,f_2}}
\end{aligned}
$$

where the step from the first line to the second line holds due to the basic property of min-plus convolution (see Rule 7 of Theorem 3.1.5 in [18]). By applying Theorem 3.1.11 in [18], the last line holds.

Similarly, we can prove that

$$\beta^l_{FC,R_{14},f_2} = \overline{\beta^l_{LT} \otimes \beta^l_{R_{13},f_2} \otimes \delta_\sigma + B_{R_{13},f_2}} \otimes \beta^l_{FC,R_{13},f_2},$$

$$\beta^l_{FC,R_{15},f_2} = \overline{\beta^l_{LT} \otimes \beta^l_{R_{14},f_2} \otimes \delta_\sigma + B_{R_{13},f_2}} \otimes \beta^l_{FC,R_{14},f_2},$$

$$\beta^l_{FC,NI,f_2} = \overline{\beta^l_{LT} \otimes \beta^l_{R_{15},f_2} \otimes \delta_\sigma + B_{R_{15},f_2}} \otimes \beta^l_{FC,R_{15},f_2}.$$

Then, the equivalent feedback service curve obtained by f_2 is

$$
\begin{aligned}
\beta^l_{f_2} &= \beta^l_{NI,f_2} \otimes \beta^l_{FC,NI,f_2} \otimes \left(\bigotimes_{R_j \in \mathcal{R}_2} (\beta^l_{R_j,f_2} \otimes \beta^l_{FC,R_j,f_2} \otimes \beta^l_{LT}) \right) \\
&= \beta^l_{NI,f_2} \otimes \left(\beta^l_{LT} \otimes \left(\bigotimes_{R_j \in \mathcal{R}_2} \beta^l_{R_j,f_2} \right) \right) \otimes \left(\beta^l_{FC,NI,f_2} \otimes \left(\bigotimes_{R_j \in \mathcal{R}_2} \beta_{FC,R_j,f_2} \right) \right) \\
&= \beta^l_{NI,f_2} \otimes \left(\beta^l_{LT} \otimes \left(\bigotimes_{R_j \in \mathcal{R}_2} \beta^l_{R_j,f_2} \right) \right) \otimes \left(\bigotimes_{R_j \in \mathcal{R}_2} \overline{\beta_{R_j,f_2} \otimes \beta_{LT} \otimes \delta_\sigma + B_{R_j,f_2}} \right) \\
&= \beta^l_{NI,f_2} \otimes \left(\bigotimes_{R_j \in \mathcal{R}_2} (\beta^l_{R_j,f_2} \otimes \beta^l_{LT} \otimes \overline{\beta^l_{LT} \otimes \beta^l_{R_j,f_2} \otimes \delta_\sigma + B_{R_j,f_2}}) \right)
\end{aligned}
$$

18

where the second line and the fourth line hold due to the commutativity of min-plus convolution, and the third line holds due to the basic property of sub-additive closure (see Corollary 3.1.1 in [18]).

490   According to the isotonicity of min-plus convolution (see Theorem 3.1.7 in [18]), we know that

$$\beta^l_{R_j,f_2} \otimes \beta^l_{LT} \otimes \overline{\beta^l_{R_j,f_2} \otimes \beta^l_{LT} \otimes \delta_\sigma(t) + B_{R_j,f_2}} \geq \beta^l_{R_j,f_2} \otimes \beta^l_{LT}, \forall R_j \in \mathcal{R}_2 \quad (6)$$

is a sufficient condition for

$$\beta^l_{f_2} \geq \beta^l_{NI,f_2} \otimes (\bigotimes_{R_j \in \mathcal{R}_2} (\beta^l_{R_j,f_2} \otimes \beta^l_{LT}))$$

where the right side is the equivalent end-to-end feed-forward service curve provided to f_2. Thus, to avoid flow control, the buffer size at each router reserved for flow f_2 can be assigned to the minimum integer value to make Eq.6 495 hold, which ends the proof. ∎

     Suppose that the applications have been mapped onto the NoC, and each flow f_i has been assigned to their corresponding priority P_i and deadline D_i. Following the same notation as Algorithm 2, we propose the buffer sizing algorithm to allocate just enough buffer for each flow to meet their deadline constraint, as 500 shown in Algorithm 3. We assume that the service curve provided by the source NI of f_i,i.e. $< \beta^l_{NI,f_i}, \beta^u_{NI,f_i} >$, has been computed with Algorithm 1.

     Our algorithm tries to reduce the buffer size for each flow from high-priority to low-priority iteratively. For each iteration, it performs the following four steps: (1) Calculate the equivalent feed-forward service curves provided by the 505 routers (lines 3-4). (2) Calculate the minimum buffer size that can avoid flow control for each router (line 5). (3) Reduce the initial buffer size gradually as long as the constraint of deadline is not being violated (line 7). This step is abstracted as a procedure Buffer_Reduction(). The Buffer_Reduction(f_i) procedure reduces the buffer size of each router reserved for the target flow f_i from 510 the ejection router to the injection router. For each router, it tries to decrease the buffer size iteratively, until the buffer size is reduced to one or the deadline constraint is violated. If the iteration stops due to the violation of deadline, the buffer size and related service curves are restored to their previous value. To ease the description, we define the operator $Pre(R_j)$ to identify the predecessor 515 of router R_j, and let $Pre(start_i) = NI$. (4) Calculate the leftover service curve at each router for low-priority flows (lines 8-23). The computation complexity of Buffer_Reduction() and the entire buffer sizing algorithm are $O(H^2)$ and $O(NH^2)$, where N and H denote the number of flows analyzed and the maximum hop count of these flows. This algorithm can be implemented in RTC 520 toolbox [21] to optimize the buffer size automatically.

     The number of cycles that a packet can be delayed in the network without violating the deadline is referred to 'slack'. Our buffer sizing algorithm reduces the buffer size iteratively as long as the slack is greater than zero, which can be used to reduce the router area and power consumption. However, while

---
Algorithm 3 Buffer sizing algorithm

Require: Architecture parameters and flow specifications
Ensure: Optimized buffer size

1: **for** each flow $f_i \in \mathcal{F}$ with priority order **do**
2:      **for** each router $R_j \in \mathcal{R}_i$ **do**
3:          $\beta^l_{FC,R_j,f_i} = \delta_0(t)$; $\beta^u_{FC,R_j,f_i} = \delta_0(t)$;
4:          $\beta^l_{R_j,f_i} = \beta^l_{BW} \otimes \beta^l_{RC} \otimes \beta^l_{VA} \otimes \beta^l_{SA} \otimes \lfloor \frac{\beta^{l'}_{ST,R^p_j}}{|\Theta_{R_j,f_i}|+1} \rfloor \otimes \beta^l_{FC,R_j,f_i}$;
5:          $\beta^u_{R_j,f_i} = \beta^u_{BW} \otimes \beta^u_{RC} \otimes \beta^u_{VA} \otimes \beta^u_{SA} \otimes \lceil \frac{\beta^{u'}_{ST,R^p_j}}{|\Theta_{R_j,f_i}|+1} \rceil \otimes \beta^u_{FC,R_j,f_i}$;
6:          compute the initial buffer size B_{R_j,f_i} according to Theorem 3;
7:      **end for**
8:      $\beta^l_{FC,NI,f_i} = \delta_0(t)$; $\beta^u_{FC,NI,f_i} = \delta_0(t)$;
9:      Buffer_Reduction(f_i);   ▷ Invoke the buffer reduction procedure
10:      $\beta^l_{f_i} = \beta^l_{NI,f_i} \otimes \beta^l_{FC,NI,f_i}$; $\beta^u_{f_i} = \beta^u_{NI,f_i} \otimes \beta^u_{FC,NI,f_i}$;
11:      **for** $\forall R_j \in \mathcal{R}_i$ from $start_i$ to end_i **do**
12:          **if** $\Omega_{R_j,f_i} \neq \emptyset$ **then**
13:              $\beta^l = \beta^l_{f_i} \otimes \beta^l_{BW} \otimes \beta^l_{RC} \otimes \beta^l_{VA} \otimes \beta^l_{SA}$;
14:              $\beta^u = \beta^u_{f_i} \otimes \beta^u_{BW} \otimes \beta^u_{RC} \otimes \beta^u_{VA} \otimes \beta^u_{SA}$;
15:              $\alpha^l_{R_j,f_i} = \min\{(\alpha^l_{f_i} \oslash \beta^u) \otimes \beta^l, \beta^l\}$;
16:              $\alpha^u_{R_j,f_i} = \min\{(\alpha^u_{f_i} \otimes \beta^u) \oslash \beta^l, \beta^u\}$;
17:              **if** $\forall f_k \in \Theta_{R_j,f_i}$, $Delay(f_k)$ has been calculated **then**
18:                  $\alpha^l_{R_j,f_i} = \alpha^l_{R_j,f_i} + \sum_{f_k \in \Theta_{R_j,f_i}} \alpha^l_{R_j,f_k}$;
19:                  $\alpha^u_{R_j,f_i} = \alpha^u_{R_j,f_i} + \sum_{f_k \in \Theta_{R_j,f_i}} \alpha^u_{R_j,f_k}$;
20:                  $\beta^{l'}_{ST,R^p_j} = (\beta^{l'}_{ST,R^p_j} - \alpha^u_{R_j,f_i}) \bar{\oslash} 0$;
21:                  $\beta^{u'}_{ST,R^p_j} = \max\{(\beta^{u'}_{ST,R^p_j} - \alpha^l_{R_j,f_i}) \bar{\oslash} 0, 0\}$;
22:              **end if**
23:          **end if**
24:          $\beta^l_{f_i} = \beta^l_{f_i} \otimes \beta^l_{R_j,f_i} \otimes \beta^l_{LT}$; $\beta^u_{f_i} = \beta^u_{f_i} \otimes \beta^u_{R_j,f_i} \otimes \beta^u_{LT}$;
25:      **end for**
26: **end for**
---

used for power reduction, it is significantly different from the DNC based slack optimization algorithm proposed in [31]. In [31], the energy optimization is achieved by adjusting the voltage, frequency and link bandwidth of on-chip routers for the fixed configuration and deadline. In contrast, our method tries to optimize the buffer size under the deadline constraint, and the buffer reduction directly leads to the area and power saving. In addition, our algorithm can be used in conjunction with the priority sharing techniques [30] to minimize the hardware cost of priority-aware wormhole-switched NoC.

1: **procedure** BUFFER_REDUCTION(f_i)
2:      **for** each router $R_j \in \mathcal{R}_i$ from end_i to $start_i$ **do**
3:         $Delay(f_i) = H(\alpha_{f_i}^u, \beta_{NI,f_i}^l \otimes \beta_{FC,NI,f_i}^l \otimes (\bigotimes\limits_{R_k \in \mathcal{R}_i} (\beta_{R_k,f_i}^l \otimes \beta_{LT}^l)));$
4:         **while** $Delay(f_i) \leq D_i$ and $B_{R_j,f_i} > 1$ **do**
5:            $B_{R_j,f_i} = B_{R_j,f_i} - 1;$
6:            **for** all $R_k \in \mathcal{R}_i$ from $Pre(R_j)$ to $start_i$ **do**
7:               compute $< \beta_{FC,R_k,f_i}^l, \beta_{FC,R_k,f_i}^u >$ according to Theorem 2;
8:               compute the service curve $< \beta_{R_k,f_i}^l, \beta_{R_k,f_i}^u >;$
9:            **end for**
10:            compute the service curve $< \beta_{FC,NI,f_i}^l, \beta_{FC,NI,f_i}^u >;$
11:            $Delay(f_i) = H(\alpha_{f_i}^u, \beta_{NI,f_i}^l \otimes \beta_{FC,NI,f_i}^l \otimes (\bigotimes\limits_{R_k \in \mathcal{R}_i} (\beta_{R_k,f_i}^l \otimes \beta_{LT}^l)));$
12:         **end while**
13:         **if** $Delay(f_i) > D_i$ **then**
14:            $B_{R_j,f_i} = B_{R_j,f_i} + 1;$
15:            recompute $< \beta_{FC,Pre(R_j),f_i}^l, \beta_{FC,Pre(R_j),f_i}^u >;$
16:            recompute $< \beta_{Pre(R_j),f_i}^l, \beta_{Pre(R_j),f_i}^u >$ if $R_j \neq start_i;$
17:         **end if**
18:      **end for**
19: **end procedure**

5. Experiments

In this section, we validate the correctness and tightness of our performance model by comparing with simulation results and other analytical methods. Several analytical methods exist for the delay analysis of priority-aware NoC, examples include contention tree model [9], lumped link model [10], dependency graph model [11], FLA [6], LLA [7] and DNC [8], etc. There are also extensive research on the buffer sizing problem of the priority-aware NoC, representative methods include shaping delay analysis [32] and LLBA [13]. Among all these analytical methods, DNC [8] and LLBA[13] based models outperform the others when the tightness of delay bound and buffer requirement is considered. Thus, we will only perform the comparison with LLBA and DNC, as presented in subsection 5.1 and subsection 5.2 respectively. We also present the simulation results to validate the correctness and tightness of our method in subsection 5.3.

The traffic pattern we discuss in this section is shown in Fig. 1. There are four flows (i.e. f_1, f_2, f_3 and f_4) in the network, with different priorities $P_4 > P_1 > P_2 > P_3$. The packet length (in flits) and injection period (in cycles) of flow f_i ($i = 1, 2, 3, 4$) are denoted as F_i and I_i, respectively. To simplify our discussion, we assume that all these four flows have the same packet length and injection period.

5.1. Comparison with Link Level Buffer-space Analysis

We perform the comparison on a set of periodical traffic due to the restriction of LLBA method [13]. To ease the analysis of buffer requirement, the LLBA method assumes the number of bits in a flit is the same as the physical channel width, and the latency of a router is one cycle [13]. Thus, our performance model for the standard wormhole-switched router should be specialized, which is achieved by letting the service curve of BW, RC, VA, SA and LT stage be a pair of burst delay function $< \delta_0(t), \delta_0(t) >$. Under this condition, the service curve of the entire router is equal to the service curve provided by the ST stage, which is $< \beta^l_{ST,R^p_i}, \beta^u_{ST,R^p_i} >$. The traffic jitter for all the flows are assumed to be zero for brevity and clarity. In addition, we set the credit feedback delay $\sigma = 0$ cycle in our model since the LLBA method does not consider the influence of credit feedback delay on the buffer requirement.

Let us suppose that all the flows have the same packet injection period $I_i = 50$ cycles and packet length $F_i = 8$ flits $(i = 1, 2, 3, 4)$. The delay bounds computed with the LLA method [7] for these four flows are 21, 22, 21 and 13 cycles, respectively. We can also obtain the total buffer size reserved for the four flows (i.e. f_1, f_2, f_3 and f_4) with LLBA method, which are 11, 12, 18 and 4 flits, respectively. The total buffer size required by these four flows can be obtained by summing up the buffer size reserved for each flow along its path, which is 45 flits. The LLBA method [13] can only give the required buffer size at each VC to avoid the back-pressure caused by flow control. By allowing the flow control to be triggered, our buffer sizing algorithm can be utilized to reduce the buffer size further as long as the deadline constraint is not violated. If we change the deadline constraint from 30 cycles to 52 cycles in step increments of 2 cycles, the total buffer size required for all the flows to meet their deadlines can be obtained by applying our buffer sizing algorithm, as shown in Fig. 6. It can be found that as the deadline increase, our method can significantly reduce the required buffer. Take the deadline $D_i = 52$ cycles as an example, our buffer sizing algorithm reduces the buffer requirement computed with the LLBA method by up to $(45 - 20)/45 \approx 55.56\%$.

5.2. Comparison with Network Calculus based Delay Analysis

In this subsection, we present the numerical results to demonstrate the improvement of our method over the DNC method proposed in [8]. The router architecture we considered in this subsection adopts the lookahead pipeline [24], which removes the RC stage from the critical path of the router pipeline. Thus, our service model is customized by letting the service curve of RC stage to be $< \delta_0(t), \delta_0(t) >$. The RTC arrival curve $< \alpha^l_{f_i}, \alpha^u_{f_i} >$ of flow f_i can be obtained according to the method introduced in subsection 4.1. The DNC arrival curve is $\alpha_{f_i} = V_i t + F_i$, where $V_i = F_i/I_i$ represents the average arrival rate. We assume the VC buffer size of each router is 32 flits, and the credit feedback delay $\sigma = 0$ cycle. We change the injection rate V_i $(i = 1, 2, 3, 4)$ from 1/3 to 1/6 (flits/cycle) and the packet length F_i from 1 to 8 flits. The end-to-end delay of flow f_3 calculated with the DNC method and our method are compared in Fig.
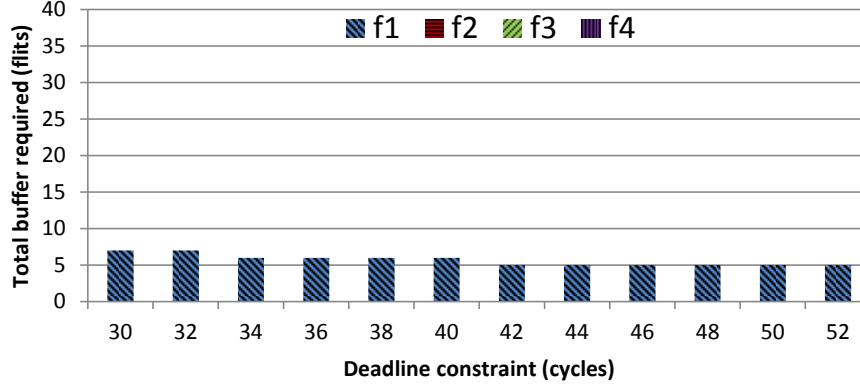
Figure 6: Buffer requirement computed with RTC model for different deadline

7. By comparison, we find that our method can give a much tighter delay bound than the DNC method proposed in [8]. The root cause for this improvement lies in the fact that our method utilizes the upper service curve to limit the output upper arrival curve, and lead to a tighter leftover service curve for the low-priority flows.

5.3. Comparison with Simulation

Our performance is verified by simulation. We modified the Booksim 2.0 [33], a cycle-accurate NoC simulator, to support the specified traffic pattern and injection process we discussed in this subsection. The traffic patterns investigated in this section include the example shown in Fig. 1 and an real application provided by Ericsson Radio Systems and discussed in [34][35]. We adopt the optimized lookahead router [24] to construct the mesh network. To fit this optimization, our service model is customized by letting the service curve of RC stage be $< \delta_0(t), \delta_0(t) >$. Other architecture and simulation parameters used in the simulation are listed in the Table 1.

Table 1: Architecture parameters used in the simulation

network topology	4×4 mesh	routing algorithm	X-Y routing
credit delay	0 cycle	channel width	128 bits
buffer size	32 flits	switch allocator	priority-based
link latency	1 cycle	sampling period	1×10^5 cycles
clock cycle	1 ns	warmup period	3×10^5 cycles

The injection process we considered in this subsection is the strictly periodical traffic without any jitter. However, even under this assumption, determining the worst-case delay by simulation for general scenarios is still a non-trivial task, because the worst-case delay of each flow depend on the traffic pattern and offset (i.e. the injection time of the first packet in a flow) of all the flows in the
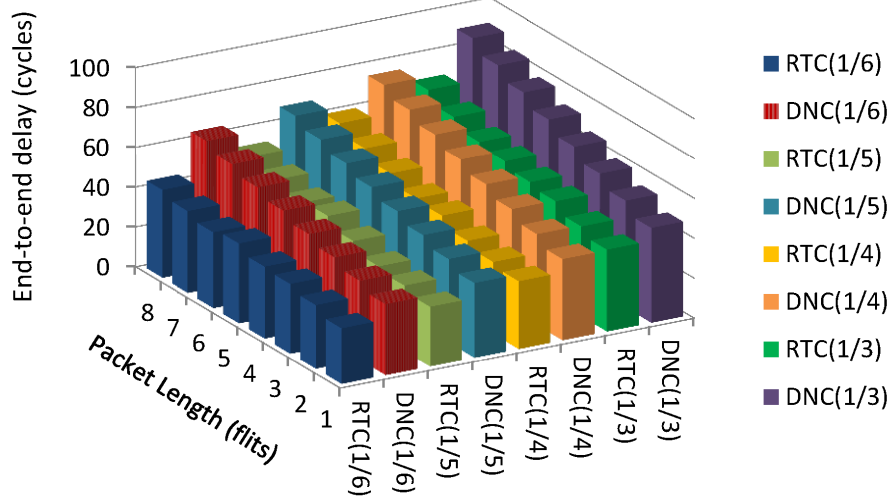
23

Figure 7: Delay bound comparison with network calculus under different injection rate and packet length

network. For the given traffic pattern shown in Fig. 1, we assume the injection rate $V_i \leq 1/3$. Under this assumptions, we find that f_1 will experience the maximum delay in the network if its offset (denoted as O_1) is equal to that of f_4. Similarly, f_2 experiences the maximum delay when its offset $O_2 = O_1 + (4+1)$, where $O_1 + (4+1)$ is the time instance that the first packet of f_1 arrives at $R_1 5$. f_3 experiences the worst-case delay when $O_3 = O_2 + F_1 + 2 \times (4+1)$. We set the injection rate V_i $(i = 1, 2, 3, 4)$ to 1/6 (flits/cycle), and change the packet length F_i from 2 flits to 9 flits. The collected maximum end-to-end delay of these four flows under the given offset combination are compared with our RTC method, as shown in Fig. 8. To prevent the results of flow f_2 from shading the results of f_3, we exchange the order of f_3 and f_4 in this figure. As indicated in the comparison, for the given configuration, delay calculated with our method is indeed an upper bound of the simulation results, which verifies the correctness of our method.

We also take an real application discussed in [34][35] as an example to demonstrate the tightness and ability of our method to analyze complex scenarios. This application is comprised of 16 IP cores. The 26 communication flows among these 16 IPs are classified into nine groups, and each group has their bandwidth requirement. When mapped to a 4×4 mesh network, the traffic pattern of this application is demonstrated in Fig. 9(a). We assume that all the flows in a group send packets periodically with the same injection period and priority, as listed in Table. 9(b). We set the packet size to 128 bits, and collect the maximum end-to-end delay of each flow obtained by simulation. The comparison results between one simulation run and the delay bound calculated with our method are shown in Fig. 10. The offset of each flow in this simulation
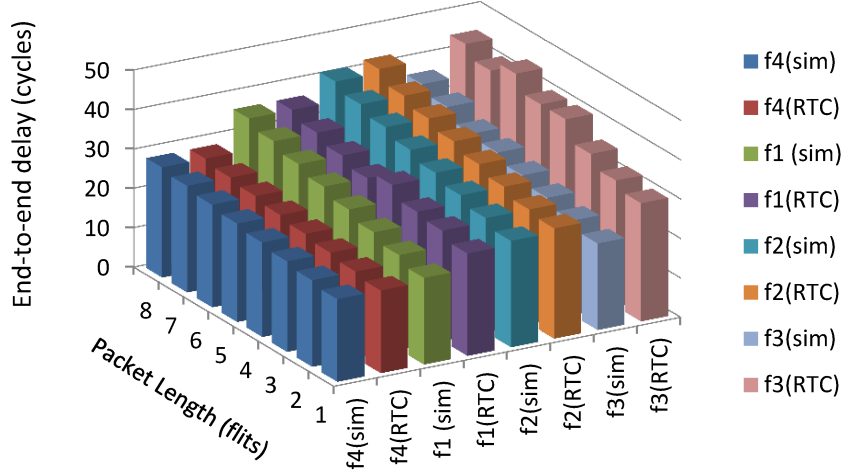
24

Figure 8: Delay comparison with simulation under different packet length

run is zero cycle. We can see that the calculated delay bounds constrain the simulation results well, which verifies the correctness of our method. This comparison also demonstrates the ability of our method to analyze the real system with large number of flows.

6. Conclusion

The priority-aware wormhole-switched NoC is a promising platform for the on-chip real-time communication if the worst-case performance can be accurately analyzed and guaranteed. Simulation is not well suited for this purpose because it is difficult to cover all the corner cases. In this paper, we proposed an RTC-based performance model to achieve this goal. We first built the traffic model and service model for the priority-aware NoC, and then proposed a novel method to derive the upper service curve of credit-based flow control. Based on the proposed RTC model, we then proposed an end-to-end delay analysis algorithm and a buffer sizing algorithm. The delay analysis algorithm can be implemented to compute the end-to-end delay for each flow automatically, and verify whether all these flows meet their deadline under the given configuration. Compared with the DNC-based performance model, our model can give tighter delay bound since it takes the upper service curve and lower arrival curve into consideration. The proposed buffer sizing algorithm can optimize the buffer size from high-priority flows to low-priority flows. It can also be implemented to perform the buffer reduction automatically under the constraint of deadline. Compared with the LLBA method which assumes the the buffer is large enough to avoid back-pressure caused by flow control, our performance model is more general. Experimental results also illustrate that our method indeed outperforms the other analytical methods, e.g. LLBA and DNC, when the tightness of
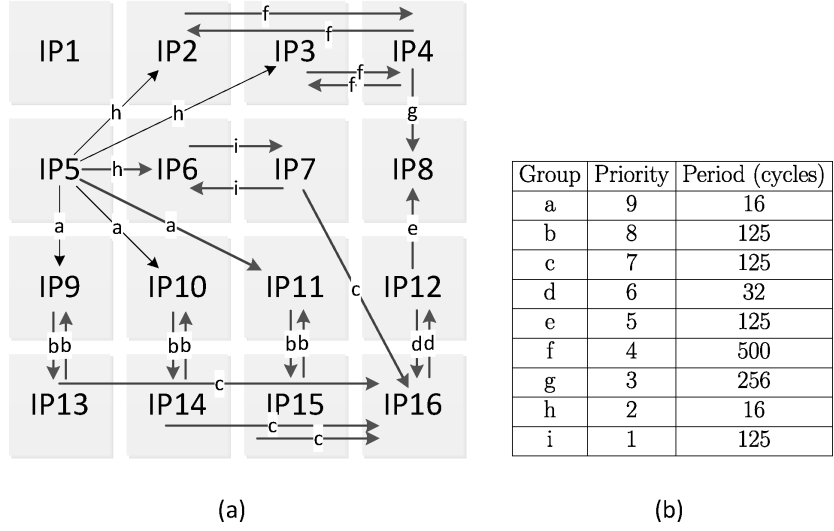
25

Figure 9: Traffic pattern of ericsson radio system application
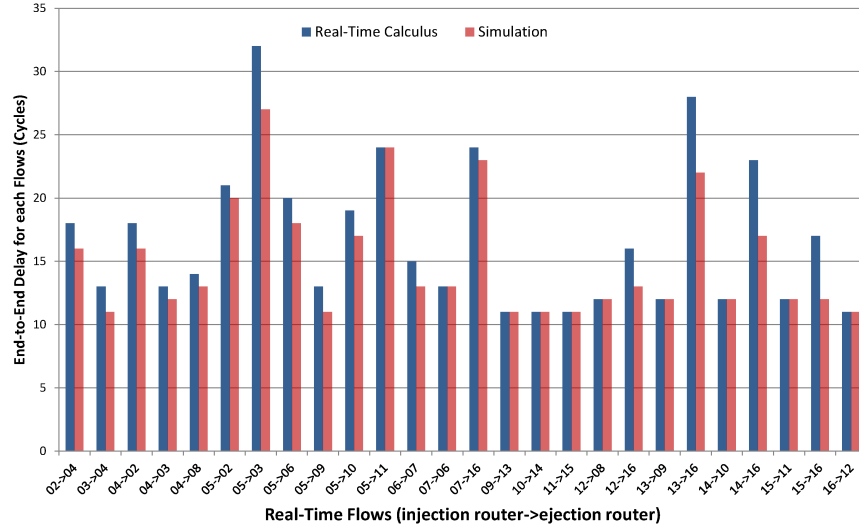

Figure 10: Delay comparison with simulation

delay bound and buffer requirement are considered. Our method can be applied to the task mapping, routing and power reduction of priority-aware NoC.

Acknowledgement

References

[1] K. Goossens, J. Dielissen, A. Radulescu, Æthereal network on chip:concepts, architectures, and implementations, IEEE Design & Test of Computers 22 (5) (2005) 414–421. `doi:http://doi.ieeecomputersociety.org/10.1109/MDT.2005.99`.

[2] S. Liu, A. Jantsch, Z. Lu, Analysis and evaluation of circuit switched noc and packet switched noc, in: Digital System Design (DSD), 2013 Euromicro Conference on, 2013, pp. 21–28. `doi:10.1109/DSD.2013.13`.

[3] C. Paukovits, H. Kopetz, Concepts of switching in the time-triggered network-on-chip, in: Embedded and Real-Time Computing Systems and Applications, 2008. RTCSA '08. 14th IEEE International Conference on, 2008, pp. 120–129. `doi:10.1109/RTCSA.2008.18`.

[4] P. Kundu, On-die interconnects for next generation cmps, in: 2006 Workshop on On- and Off-Chip Interconnection Networks for Multicore Systems, Stanford, CA, USA, 2006.

[5] G. Michelogiannakis, D. Sanchez, W. Dally, C. Kozyrakis, Evaluating bufferless flow control for on-chip networks, in: Networks-on-Chip (NOCS), 2010 Fourth ACM/IEEE International Symposium on, 2010, pp. 9–16. `doi:10.1109/NOCS.2010.10`.

[6] Z. Shi, A. Burns, Real-time communication analysis for on-chip networks with wormhole switching, in: Proceedings of the Second ACM/IEEE International Symposium on Networks-on-Chip (NoCs), 2008, IEEE Computer Society, Washington, DC, USA, 2008, pp. 161–170.

[7] H. Kashif, H. D. Patel, S. Fischmeister, Using link-level latency analysis for path selection for real-time communication on nocs, in: Proceedings of the Asia South Pacific Design Automation Conference (ASPDAC), Sydney, Australia, 2012, pp. 499–504. `doi:10.1109/ASPDAC.2012.6165004`.

[8] Y. Qian, Z. Lu, Q. Dou, Qos scheduling for nocs: Strict priority queueing versus weighted round robin, in: Computer Design (ICCD), 2010 IEEE International Conference on, 2010, pp. 52–59. `doi:10.1109/ICCD.2010.5647577`.

[9] Z. Lu, A. Jantsch, I. Sander, Feasibility analysis of messages for on-chip networks using wormhole routing, in: Design Automation Conference, 2005. Proceedings of the ASP-DAC 2005. Asia and South Pacific, Vol. 2, 2005, pp. 960–964 Vol. 2. `doi:10.1109/ASPDAC.2005.1466499`.

[10] S. Balakrishnan, F. Özgüner, A priority-driven flow control mechanism for real-time traffic in multiprocessor networks, IEEE Trans. Parallel Distrib. Syst. 9 (7) (1998) 664–678. `doi:10.1109/71.707545`.

[11] B. Kim, J. Kim, S. Hong, S. Lee, A real-time communication method for wormhole switching networks, in: Parallel Processing, 1998. International Conference on, 1998, pp. 527–534. `doi:10.1109/ICPP.1998.708526`.

[12] S. Chakraborty, S. Kunzli, L. Thiele, A general framework for analysing system properties in platform-based embedded system designs, in: Design, Automation and Test in Europe Conference and Exhibition, 2003, 2003, pp. 190–195. `doi:10.1109/DATE.2003.1253607`.

[13] H. Kashif, H. Patel, Bounding buffer space requirements for real-time priority-aware networks, in: Design Automation Conference (ASP-DAC), 2014 19th Asia and South Pacific, 2014, pp. 113–118. `doi:10.1109/ASPDAC.2014.6742875`.

[14] W. J. Dally, B. Towles, Route packets, not wires: On-chip interconnection networks, in: Proceedings of the 38th Design Automation Conference, 2001, pp. 684–689.

[15] E. Bolotin, I. Cidon, R. Ginosar, A. Kolodny, Qnoc: Qos architecture and design process for network on chip, J. Syst. Archit. 50 (2-3) (2004) 105–128. `doi:10.1016/j.sysarc.2003.07.004`.

[16] Z. Shi, Real-time communication services for networks on chip, Ph.D. thesis, The University of York (2009).

[17] Y. Qian, Z. Lu, W. Dou, Analysis of worst-case delay bounds for best-effort communication in wormhole networks on chip, in: Networks-on-Chip (NoCs), 2009. 3rd ACM/IEEE International Symposium on, 2009, pp. 44–53. `doi:10.1109/NOCS.2009.5071444`.

[18] J.-Y. Le Boudec, P. Thiran, Network Calculus: A Theory of Deterministic Queuing Systems for the Internet, Springer-Verlag, Berlin, Heidelberg, 2001.

[19] D. Chokshi, P. Bhaduri, Modeling fixed priority non-preemptive scheduling with real-time calculus, in: Embedded and Real-Time Computing Systems and Applications, 2008. RTCSA '08. 14th IEEE International Conference on, 2008, pp. 387–392. `doi:10.1109/RTCSA.2008.28`.

[20] A. Hagiescu, U. D. Bordoloi, S. Chakraborty, P. Sampath, P. V. V. Ganesan, S. Ramesh, Performance analysis of flexray-based ecu networks, in: Proceedings of the 44th Annual Design Automation Conference, DAC '07, ACM, New York, NY, USA, 2007, pp. 284–289. `doi:10.1145/1278480.1278554`.

[21] E. Wandeler, L. Thiele, Real-time calculus (rtc) toolbox, http://www.mpa.ethz.ch/Rtctoolbox (2006).

[22] S. Hary, F. Ozguner, Feasibility test for real-time communication using wormhole routing, Computers and Digital Techniques, IEE Proceedings - 144 (5) (1997) 273–278. `doi:10.1049/ip-cdt:19971369`.

[23] W. J. Dally, B. Towles, Principles and Practices of Interconnection Networks, Morgan Kaufman Publishers, San Francisco, CA, USA, 2004.

[24] N. Jerger, L. Peh, On-chip networks, Synthesis Lectures on Computer Architecture 4 (1) (2009) 1–141.

[25] W. Dally, S. Tell, The even/odd synchronizer: A fast, all-digital, periodic synchronizer, in: Asynchronous Circuits and Systems (ASYNC), 2010 IEEE Symposium on, 2010, pp. 75–84. `doi:10.1109/ASYNC.2010.20`.

[26] S. Lee, Real-time wormhole channels, J. Parallel Distrib. Comput. 63 (3) (2003) 299–311. `doi:10.1016/S0743-7315(02)00055-2`.

[27] E. Wandeler, L. Thiele, M. Verhoef, P. Lieverse, System architecture evaluation using modular performance analysis: A case study, Int. J. Softw. Tools Technol. Transf. 8 (6) (2006) 649–667. `doi:10.1007/s10009-006-0019-5`.

[28] H. Schiøler, J. J. Jessen, J. D. Nielsen, K. G. Larsen, Network calculus for real time analysis of embedded systems with cyclic task dependencies., in: Proc. 20th International Conference on Computers and Their Applications, CATA 2005, 2005, pp. 326–332.

[29] L. Thiele, N. Stoimenov, Modular performance analysis of cyclic dataflow graphs, in: Proceedings of the Seventh ACM International Conference on Embedded Software, EMSOFT '09, ACM, New York, NY, USA, 2009, pp. 127–136. `doi:10.1145/1629335.1629353`.

[30] Z. Shi, A. Burns, Real-time communication analysis with a priority share policy in on-chip networks, in: Real-Time Systems, 2009. ECRTS '09. 21st Euromicro Conference on, 2009, pp. 3–12. `doi:10.1109/ECRTS.2009.17`.

[31] J. Zhan, N. Stoimenov, J. Ouyang, L. Thiele, V. Narayanan, Y. Xie, Designing energy-efficient noc for real-time embedded systems through slack optimization, in: Design Automation Conference (DAC), 2013 50th ACM / EDAC / IEEE, 2013, pp. 1–6.

[32] S. Manolache, P. Eles, Z. Peng, Buffer space optimisation with communication synthesis and traffic shaping for nocs, in: Design, Automation and Test in Europe, 2006. DATE '06. Proceedings, Vol. 1, 2006, pp. 1–6. `doi:10.1109/DATE.2006.244069`.

[33] N. Jiang, D. Becker, G. Michelogiannakis, J. Balfour, B. Towles, D. Shaw, J. Kim, W. Dally, A detailed and flexible cycle-accurate network-on-chip simulator, in: Performance Analysis of Systems and Software (ISPASS), 2013 IEEE International Symposium on, 2013, pp. 86–96. `doi:10.1109/ISPASS.2013.6557149`.

[34] Z. Lu, A. Jantsch, Tdm virtual-circuit configuration for network-on-chip, Very Large Scale Integration (VLSI) Systems, IEEE Transactions on 16 (8) (2008) 1021–1034. `doi:10.1109/TVLSI.2008.2000673`.

[35] F. Jafari, Z. Lu, A. Jantsch, M. H. Yaghmaee, Buffer optimization in network-on-chip through flow regulation, Trans. Comp.-Aided Des. Integ. Cir. Sys. 29 (12) (2010) 1973–1986. `doi:10.1109/TCAD.2010.2063130`.